Supplementary Information

Promotion of Water-Mediated Carbon Removal by Nanostructured Barium Oxide/Nickel Interfaces in Solid Oxide Fuel Cells

Lei Yang[1], YongMan Choi[2], Wentao Qin[1], Haiyan Chen[3], Kevin Blinn[1], Mingfei Liu[1], Ping Liu[2], Jianming Bai[4], Trevor A. Tyson[3] & Meilin Liu[1,*]

[1] *School of Materials Science and Engineering, Center for Innovative Fuel Cell and Battery Technologies, Georgia Institute of Technology, Atlanta, GA 30332-0245, USA*
[2] *Chemistry Department, Brookhaven National Laboratory, Upton, NY 11973, USA*
[3] *Department of Physics, New Jersey Institute of Technology, Newark, NJ 07102, USA*
[4] *High Temperature Materials Laboratory, Oak Ridge National Laboratory, Oak Ridge, TN 37831, USA*
[*] Correspondence and requests for materials should be addressed to M.L.L. (email: meilin.liu@mse.gatech.edu).

Supplementary Figures

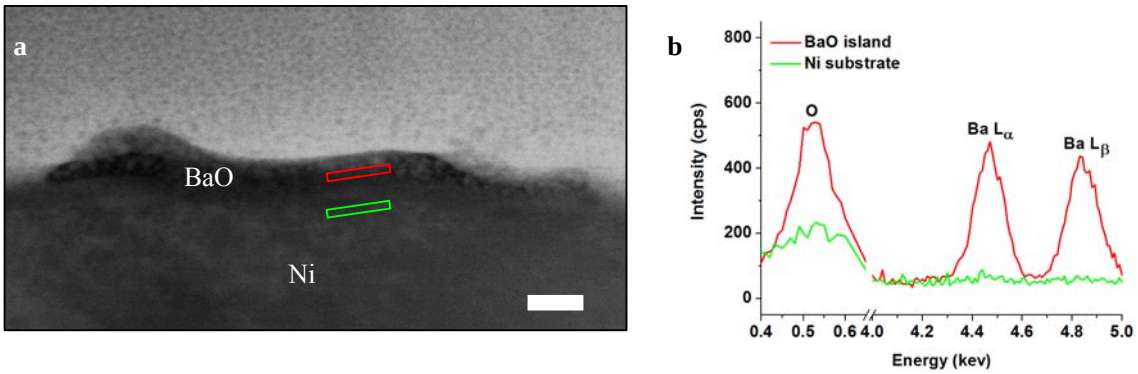

Supplementary Fig. S1. Z-contrast image (a) of a BaO/Ni interface (the scale bar is 20 nm) and EDS spectra (b) acquired from the BaO island and the underlying Ni. The EDS spectra were acquired from the rectangular areas marked in (a). It shows a Z-contrast image (a) of the BaO island shown in Fig. 1c and EDS spectra (b) acquired from the BaO island and the underlying Ni. The EDS spectra were acquired from the rectangular areas in the BaO island and the underlying Ni as marked in (a). Presence of Ba and O in the island was verified, along with the identification of Ni underneath the island, which is consistent with electron diffraction (pattern presented in Supplementary Figure S2) and lattice fringe (HRTEM images presented in Figs. 1e and 1f) analyses.

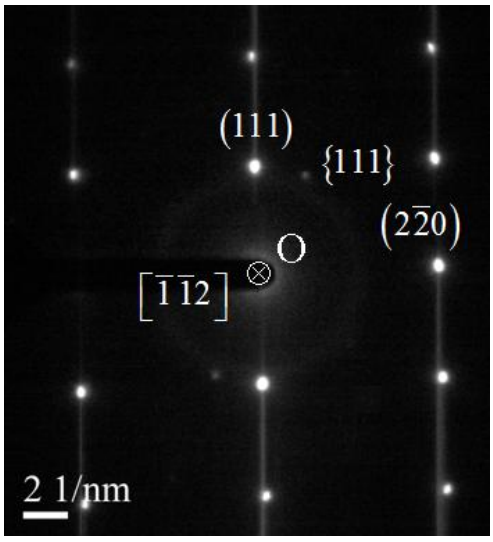

Supplementary Fig. S2. Selected area electron diffraction (SAED) pattern of the stack of Ni/BaO island/part of the tungsten coating. The Miller indices and crystallographic direction labeled are those of Ni. It shows a selected area electron diffraction (SAED) pattern of the stack of Ni/BaO island/part of the tungsten coating. All the diffraction spots can be indexed with Ni, which suggests lack of long-range order of the BaO island. This is consistent with XRD and HRTEM data presented in Figs. 1a and 1e.

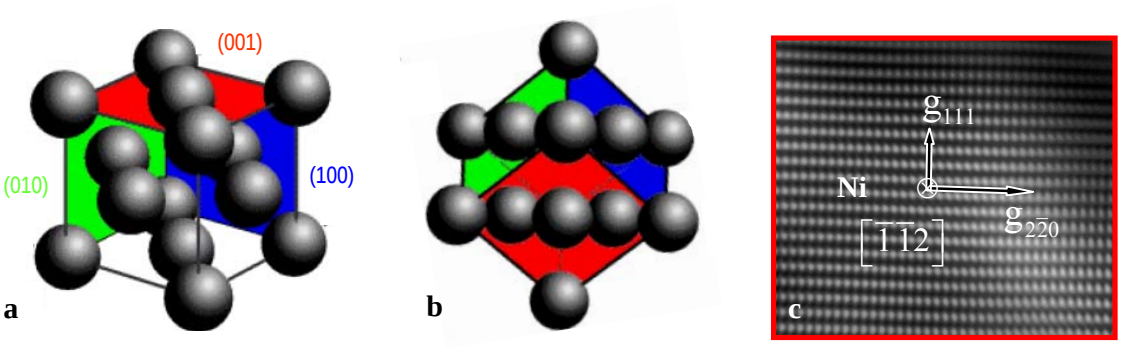

Supplementary Fig. S3. Ball models of an fcc lattice in perspective view (a) and seen along the **[** $\bar{1}\bar{1}$ 2**]** zone axis (b), and the Fourier-filtered image of the Ni immediately under the BaO island (c). The Miller indices in (a) denote the lattice planes, with each pair of indices and plane assigned the same color. It presents ball models of an fcc lattice in a "conventional" and more intuitive perspective view (a) and visualized along the **[** $\bar{1}\bar{1}$ 2**]** zone axis (b). The Fourier-filtered image of the **[** $\bar{1}\bar{1}$ 2**]** Ni grain presented in Fig. 1f is shown in Supplementary Figure S3c. Supplementary Figures S3b and S3c are identically oriented for the ease of correlation between the ball model and the information derived from the HRTEM observation.

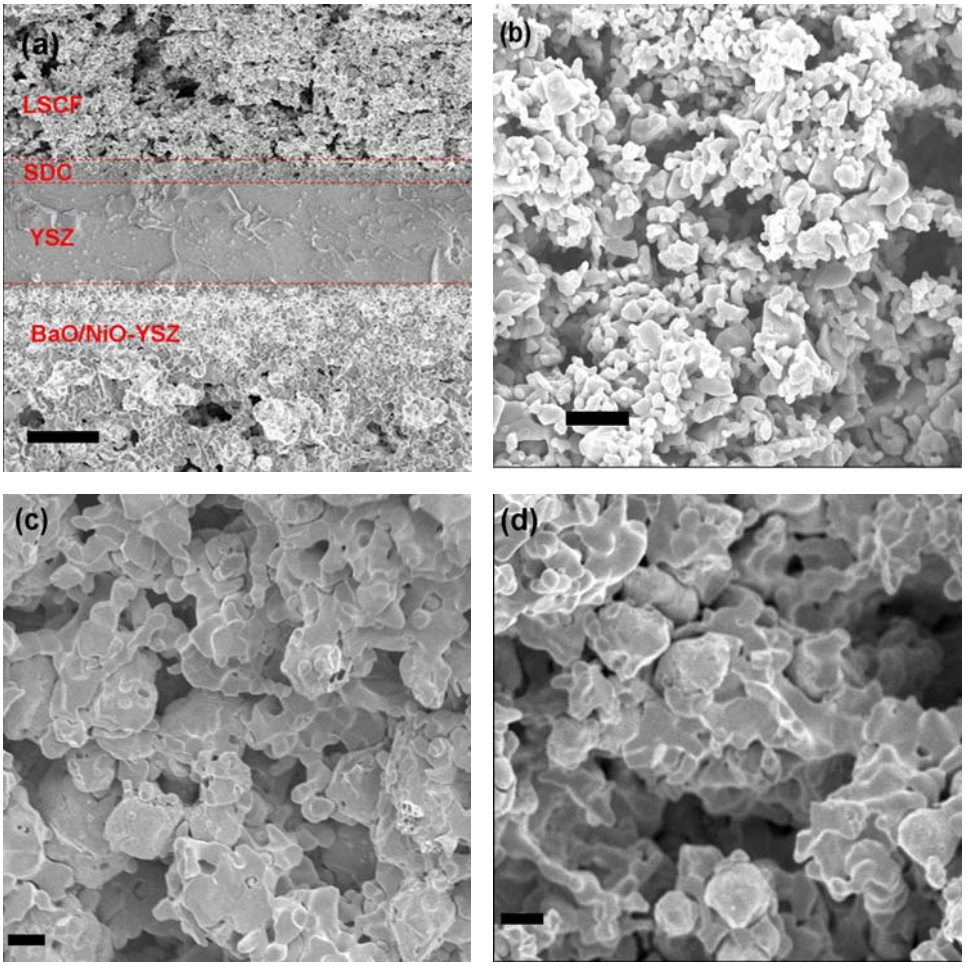

Supplementary Fig. S4. (a) A cross-sectional view (SEM image) of a cell with a configuration of BaO/Ni-YSZ |YSZ| SDC/LSCF (before NiO was reduced to Ni). The scale bar is 10 μm; (b) LSCF cathode. The scale bar is 2 μm. The BaO/Ni-YSZ anode before operation (c) and after operation (d) in C_3H_8 and gasified carbon at 750ºC (The scale bar is 2 μm). Figure S4a shows a cross-sectional view of a typical fuel cell (as fabricated) with a BaO/Ni-YSZ anode, a YSZ electrolyte, an SDC buffer layer and an LSCF cathode. The YSZ electrolyte is ~15 μm thick. To avoid formation of insulating phases between the YSZ and LSCF cathode, an SDC buffer layer (~2 μm thick) was applied to the YSZ before application of the LSCF cathode. SEM images of the BaO/Ni-YSZ anode before and after operation (Supplementary Figures 4c and 4d) at 750ºC in C_3H_8 and gasified C show no observable carbon deposits blocking the pores. While carbons deposit were largely absent on the anode, we observed the carbon deposition on the cell mounting tube walls. Since the Ni-YSZ anode normally experiences the most severe coking problem and the most rapid deactivation than other cell components, the carbon buildup on anode compartment surfaces around the cell could be readily eliminated if the same modification technique is employed. Understanding of the carbon chemistry on the anode during the electrochemical process could be implemented in the investigations of reactions occurring on the non-electrochemical-active areas (other cell components exposed in fuels), which are purely chemical processes.

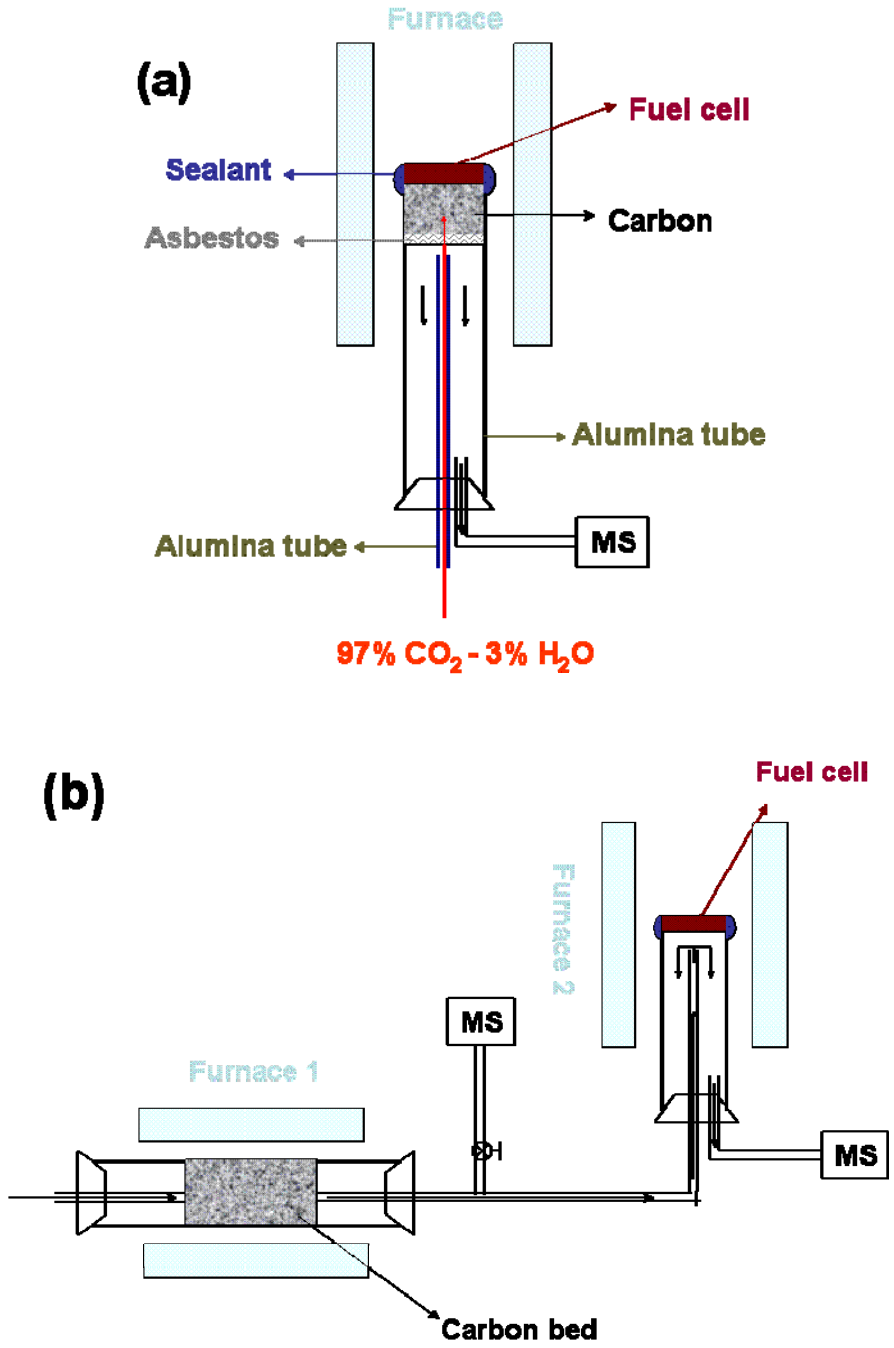

Supplementary Fig. S5. Schematic depictions of our testing systems with an integrated fluidized-bed gasifier (a) and an external fluidized-bed coupled to a fuel cell (b). Figure S5a shows schematically the configuration of a SOFC using gasified carbon in this study. It consists of an integrated fluidized bed gasifier and a single cell. Also, we investigated a design with an external gasifier coupled with a fuel cell to understand the fundamental issues (similar to a previous study by Gür et al[44]), as shown in Figure S5b. In these systems, carbon was gasified in a fluidized bed by CO_2 to CO, which was then electrochemically oxidized to CO_2 on the BaO/Ni-YSZ anode. Recycling 50% of the exhaust CO_2 back to the fluidized bed allows more efficient recovery of the waste heat of

the product stream and enhances system efficiency. With the configuration in Supplementary Figure S5b, a fuel cell also produced a similar power output at 750°C (without any carbon deposition) and the fuel utilization was about ~5%. This low fuel utilization represents a very severe condition for carbon deposition since the tendency for carbon deposition decreases with the increase in fuel utilization. If the anode displays sufficient tolerance to coking under this condition, it should not experience carbon buildup at higher fuel utilization when more oxidation products (CO_2 and H_2O) are produced in the anodic compartment.

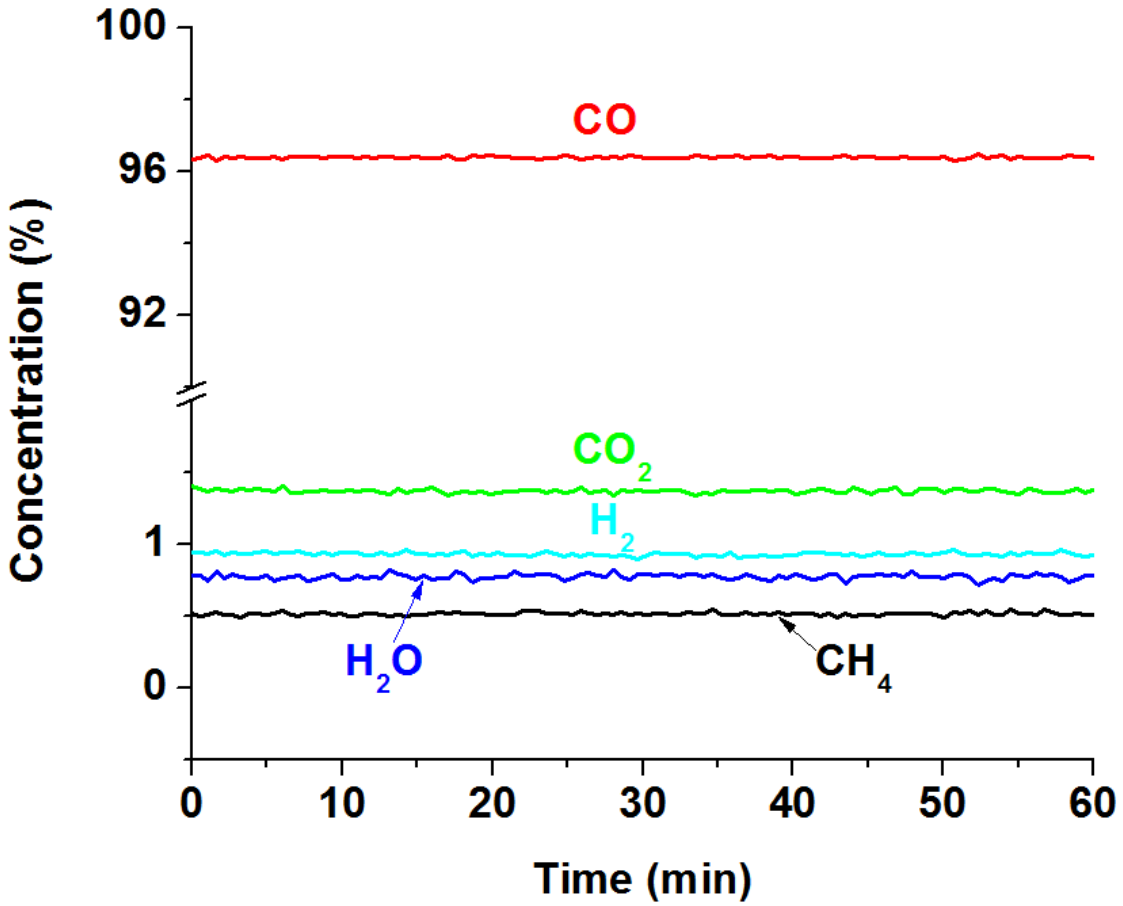

Supplementary Fig. S6. A typical concentration profile of the outlet gas mixture from the gasifier monitored using a mass spectrometer. It shows the composition of the effluent gas from the gasifier, as monitored using a mass spectrometer. The concentration of CO was relatively high and those of CO_2 and H_2O were relatively low, implying effective gasification of carbon under the operation conditions.

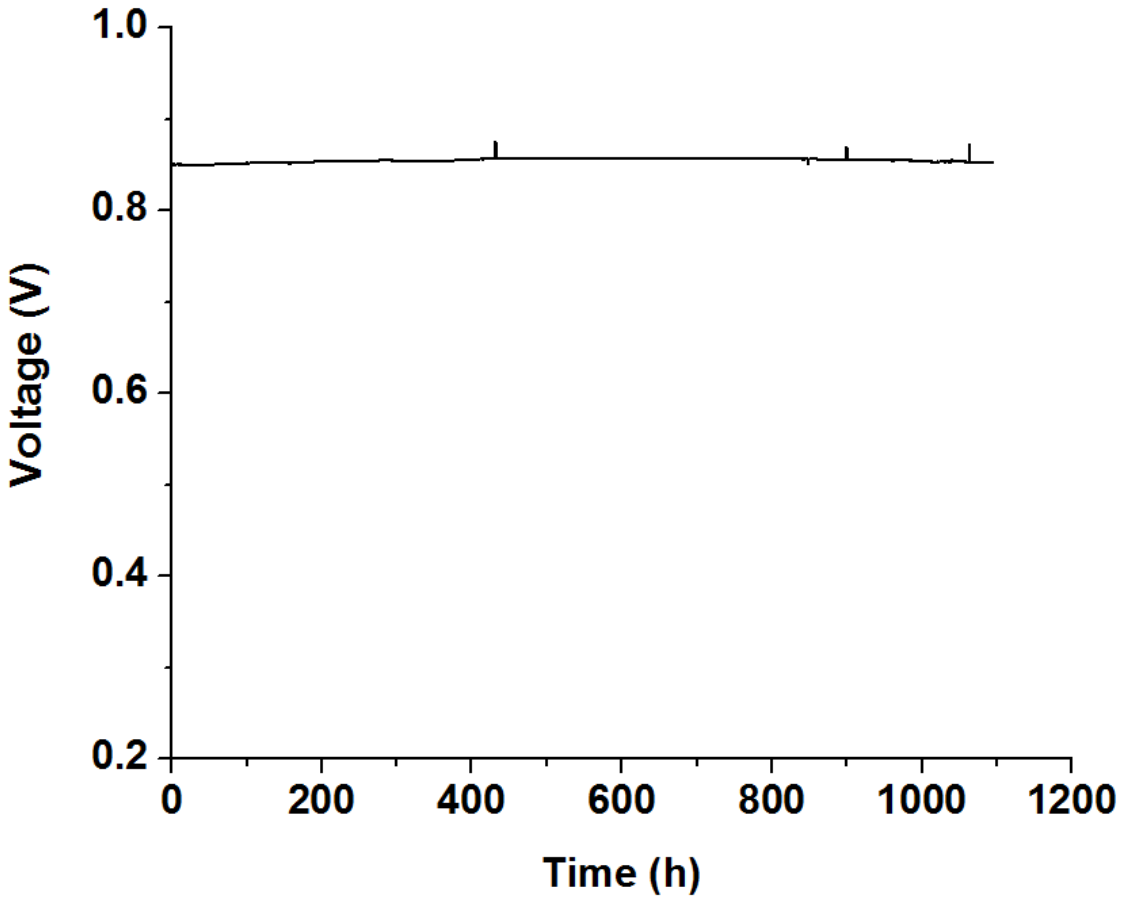

Supplementary Fig. S7. Terminal voltage for a cell with a configuration of BaO/Ni-YSZ |YSZ| SDC/LSCF and operated at 400 mA/cm^2 in dry hydrogen at 750^{o}C. It shows the terminal voltage as a function of time for a cell with a configuration of BaO/Ni-YSZ |YSZ| SDC/LSCF operated at a constant current density of 400 mA/cm^2 at 750ºC using H_2 as the fuel. This new anode can be readily incorporated into the state-of-the-art fuel cell system. The sustained power output for ~1000 h in H_2 implies that the new anode is stable for long-term operation.

Supplementary Tables

Supplementary Table S1. Comparison of power density of cells with various alternative anodes

Cell configuration	Fuel composition	Operating temperature (^oC)	Peak power density (W/cm^2)	Reference
BaO/Ni-YSZ |YSZ| SDC/LSCF	97% CO-3%H_2O	750	0.70	This study
$La_{0.8}Sr_{0.2}Sc_{0.2}Mn_{0.8}O_3$|YSZ| $La_{0.8}Sr_{0.2}Sc_{0.2}Mn_{0.8}O_3$	CO	850	0.20	Ref. 45
Pd-$La_{0.8}Sr_{0.2}Cr_{0.5}Mn_{0.5}O_3$-$Ce_{0.48}Zr_{0.48}Y_{0.04}O_2$ |YSZ| LSF-YSZ	50%CO-50%CO_2	800	0.45	Ref. 46
Cu-CeO_2-YSZ |YSZ| LSF-YSZ	CO	700	0.30	Ref. 47

Supplementary Table S2. DFT calculations of H_2O adsorption on different materials

Material	Surface	$E_{ads,H2O}$ (eV)	Adsorption Configuration	Adsorption Type
BaO	NaCl, five-layer (001)	–1.35 (1/4 ML)	atop-bound to an O ion through H	dissociative
Ni[a]	fcc, three-layer p(3 × 5) (111)	–0.32 (1/15 ML)	atop-bound through O	Molecularly
YSZ[b]	cubic, nine-layer (111)	–0.54 (1/4 ML)	atop-bound to a Zr ion through H	Molecularly

a. p(3 × 3) (111) (1/9 ML): –0.30 eV.
b. One oxygen vacancy was generated by replacing two Zr^{4+} with two Y^{3+}.

Supplementary References

44. Gür, T.M., Homel, M. & Virkar, A.V. High performance solid oxide fuel cell operating on dry gasified coal. *J. Power Sources* **195**, 1085-1090 (2010).
45. Su, C. *et al.* Assessment of nickel cermets and $La_{0.8}Sr_{0.2}Sc_{0.2}Mn_{0.8}O_3$ as solid-oxide fuel cell anodes operating on carbon monoxide fuel. *J. Power Sources* **195**, 1333-1343 (2010).
46. Bidrawn, F. *et al.* Efficient reduction of CO_2 in a solid oxide electrolyzer. *Electrochem. Solid-State Lett.* **11**, B167-B170 (2008).
47. Costa-Nunes, O., Gorte, R.J. & Vohs, J.M. Comparison of the performance of Cu-CeO_2-YSZ and Ni-YSZ composite SOFC anodes with H_2, CO, and syngas. *J. Power Sources* **141**, 241-249 (2005).